PNAS
www.pnas.org

Supplementary Information for

Context-dependent operation of neural circuits underlies a navigation behavior in *Caenorhabditis elegans*

Muneki Ikeda, Shunji Nakano, Andrew C. Giles, Linghuan Xu, Wagner Steuer Costa, Alexander Gottschalk, and Ikue Mori

Ikue Mori
Email: m46920a@nucc.cc.nagoya-u.ac.jp

This PDF file includes:

Other supplementary materials for this manuscript include the following:

www.pnas.org/cgi/doi/10.1073/pnas.1918528117

SI Materials and Methods

Strains. *C. elegans* animals were cultivated under the standard condition (1). Adult hermaphrodites were used in this study. N2 (Bristol) was the wild-type strain, and all the other strains used in this study were derived from N2.

Cell-ablated strains were generated by the expression of reconstituted caspases (2) and by mito-miniSOG with the FLP/FRT strategy (3, 4). Cell-silenced strains were generated by the expression of HisCl1 with the FLP/FRT strategy (5). Each of the plasmids expressing reconstituted caspase was injected at 25 ng/μl, each of the plasmids expressing mito-miniSOG was injected at 50–75 ng/μl, and each of the plasmids expressing HisCl1 was injected at 50 ng/μl. pKDK66 (ges-1p::NLS::GFP) (50 ng/μl) or pNAS88 (ges-1p::NLS::TagRFP) (50 ng/μl) were co-injected as an injection marker. Cell-specific expressions were achieved by using the promoter sets listed in *SI Appendix*, Table S1 and S2. Specificity was confirmed by expressing TagRFP under the listed promoter sets with the FLP/FRT strategy and also by checking the fluorescence from mito-miniSOG, HisCl1::SL2::GFP, and HisCl1::SL2::mCherry. Extrachromosomal arrays were integrated into the genome via gamma irradiation-induced mutagenesis except for *njIs127*, which was spontaneously generated through the daily maintenance, and outcrossed more than four times before analysis. PY7505 was kindly provided by Piali Sengupta, Brandeis University, MA, USA (6).

Integrants of recCaspases were crossed into integrated reporter lines listed in *SI Appendix*, Table S3 that express GFPs or TagRFPs in several neurons including the neuron of interest. Losses of neurons were confirmed at the adult stage by the disappearance of fluorescence from the target neurons. For cell ablations by mito-miniSOG, plates containing OP50 and the L1 stage animals were exposed, without any covers, to pulsed blue light (488 nm) in 0.5 sec on and 1.5 sec off cycles for 30 min. The blue light intensity received by the animals was measured as 106 mW/cm^2. Losses of neurons were confirmed at the adult stage by the disappearance of fluorescence from the miniSOG. To control the shutters, we used five spot-type deep UV lamps (SP-9250EF-N, USHIO) connected by light guide fiber units (SP-155XQ-S11, USHIO) and a control box (SP-SC-N, USHIO). The efficiencies of the cell ablations are also listed in *SI Appendix*, Table S1.

Thermotaxis Assay. Thermotaxis (TTX) assays were performed as previously described (7). Animals cultivated at 17 °C, 20 °C, or 23 °C were placed on the center of the assay plate (13.6 cm×9.6 cm, 1.45 cm height) containing 18 ml of TTX medium with 2% agar, and were allowed to freely move for 60 min. The center of the plate was adjusted at 14 °C, 17 °C, 20 °C, 23 °C, and 26 °C depending on the experiments. The plate was maintained with a linear thermal gradient of approximately 0.45 °C/cm. TTX assays with animals expressing HisCl1 were performed on 10 mM histamine-containing assay plates that were prepared as previously described (5). 1 M histamine-dihydro-chloride (Sigma-Aldrich) was added to TTX medium at ~65 °C immediately before pouring plates. The effect of cell silencing on the plates was checked by rapid (<1 min), prolonged (>60 min), and reversible paralysis of a panneural HisCl1-expressing animal, CX14370, which was kindly provided by Cornelia Bargmann, The Rockefeller University, NY, USA (5).

In TTX assays in which animals were reposition from one assay plate to another (*SI Appendix*, Fig. S4*A*), the animals were collected from the plate with 2 ml of NG buffer (0. 3% NaCl, 1 mM $CaCl_2$, 1 mM $MgSO_4$, 25 mM potassium phosphate, pH 6.0) and then placed on the center of the another plate. These steps were carried out within 3 min.

Behavioral Recording. Behavioral recordings were performed using a Multi-Worm Tracker (8, 9) with a CMOS sensor Camera Link Camera (8 bits, 4,096 × 3,072 pixels; CSC12M25BMP19-01B, Toshiba-Teli), a lens adaptor (F-TAR2), a Line-Scan Lens (35mm, f/2.8; YF3528,

PENTAX), and a PCIe-1433 camera-link frame grabber (781169-01, National Instruments). The camera was mounted at a distance above the assay plate resulting in an image with 33.2 μm per pixel. The frame rate of recordings was approx. 13.5 Hz. Images were captured and processed by custom software written in LabView (National Instruments) and a custom image analysis library written in C++, which detect animals and measure parameters such as the positions and the postures of animals.

Behavioral Analysis. The MWT system automatically identifies animals and provides the positions of their centers of mass and the 11 points along their bodies, as well as their body lengths, widths, and so on (8). Using these data, the behavioral analysis was performed with a custom-built MATLAB (MathWorks) script. For each frame, we defined the moving direction as the vectors from the current centroid to the following centroid (1 sec after), and calculated the *curve* by the angle between the previous moving direction (1 sec before) and the current moving direction. When an animal performs the *omega turn*, its head and tail become close together accompanying the decrease of the estimated body length in the system. Therefore, if the body length was estimated shorter than 1.5 standard deviation from the mean and the curve value at that time was greater than 90°/sec, we regarded the animal as performing the omega turn. To detect *shallow turns*, we defined the head swing for each frame as the angle between the vector from the 3rd point to the 1st point and the vector from the 7th point to the 5th point along the worm's body. If the head swing was over 2 standard deviation from the mean and the curve value at that time was in the range of 15–90°, we regarded the worm as performing the shallow turn. *Reversals* were detected by the smoothed curve (the moving average of the curves within three frames) which was greater than 150°/sec. If a reversal was followed by an omega turn within 6 seconds, these two components were combined into a *reversal turn* (10, 11). All the curve thresholds described above were determined following the previous proposals (12, 13).

Isothermal tracking was defined as continuous movement, which was not interrupted by any turns or reversals, toward isothermal direction ± 25° for longer than 20 sec (14). Since the thermal gradients were slightly distorted near the edges of the plates (Fig. 1*B*), isothermal direction was tilted by 5° along the distortion of the gradients (Fig. 1*D*). The fraction of isothermal tracking was calculated by summing all the durations of isothermal tracking divided by all the durations of running of animals.

Computer Simulation. Thermotaxis behavior was simulated using another custom-built MATLAB script. For each simulation, 100 animals were run sequentially. Animals were considered as dimensionless points in a 13.6 cm (x axis) × 9.6 cm (y axis) plate, with a linear thermal gradient from 14 to 20 °C, from 20 to 26 °C, or from 23 to 29 °C along the x axis. Animals started from the center of a plate, while y coordinates and initial directions were randomized. For every second, animals decided whether to undergo an omega turn, a shallow turn, a reversal, a reversal turn, or a curve (Fig. 3*A*). Event probabilities of each behavioral component were defined according to the experimental data of turning frequencies. When animals decided to do any turns, the next moving directions (θ) were defined according to the experimental data of exit directions (Φ). The next positions (x, y) were defined together with the experimental data of the displacements during the individual turns that were also calculated in MWT analysis. When animals decided to do a curve, the next moving directions θ were defined according to the experimental data of curving biases (φ). The next positions (x, y) were defined together with the experimental data of the speed. If an animal reaches the plate border, it was set to do specular reflection. When disabling each of the behavioral components, we replaced the experimental data of interest with the data taken from the animals on the constant temperature. When enabling each of the behavioral components, we replaced the experimental data of interest on the constant temperature with the data taken from the animals on the thermal gradient. Every experimental data was applied as a function of moving direction θ. Besides, different data set were applied

depending on whether the animals were on the fraction 1–2, the fraction 3–6, or the fraction 7–8 of a thermotaxis plate (Fig. 1*C*). Each simulation lasts for 30 min, and the simulations were iterated 100 times and the time courses of TTX indices were averaged within them.

Calcium Imaging in Freely Moving Animals. Ca^{2+} imaging recordings in freely moving animals were performed as previously described (15) with custom modifications. The FRET-based calcium probe yellow cameleon X 1.60 was expressed in the neuron of interest (*SI Appendix*, Table S3). A dual-view was equipped with 05-EM CFP/YFP (505 dcxr) filter cube (Molecular Devices), and images were acquired using EM-CCD camera (C9100-13, Hamamatsu Photonics) with 400 ms pulsed illumination every 1 sec (SPECTRA, Lumencor). Simultaneous tracking was performed using a CMOS camera (Grasshopper Express GX-FW-28S5M-C, FLIR Integrated Imaging Solutions) at 30 frames per second with continuous halogen illumination (TH4-100, Olympus) through an IR filter (IR-76, Fujifilm).

Calcium Imaging in Immobilized Animals. Ca^{2+} imaging recordings in immobilized animals were performed as previously described (16, 17) with custom modifications. The calcium probe GCaMP3 or GCaMP6f was expressed together with TagRFP in the neuron of interest (*SI Appendix*, Table S3). Animals were placed on a 10% agar pad on a cover slip and immobilized by 2 mM levamisole (Wako) with 0.1 μm polystyrene beads (Polysciences). The samples were covered by another cover slip and placed onto a Peltier-based temperature controller (Tokai Hit). A dual-view was equipped with OI-11-EM GFP/RFP (565 dcxr) filter cube (Molecular Devices), and images were acquired using EM-CCD camera (C9100-13, Hamamatsu Photonics) with 400 ms pulsed illumination every 1 sec (SPECTRA, Lumencor). The samples were initially kept at 15°C (or 21°C) for 5 min and then subjected to a linear temperature increase to 19°C (or 25°C) over 10 sec followed by 60 sec of incubation at 19°C (or 25°C) and a linear temperature decrease to 15°C (or 21°C) over 10 sec. Each animal was imaged two or three times, separated by a 5-min interval.

Imaging Analysis. The image processing program for the tracking data was written in MATLAB. A neuronal region was defined according to the peak intensity and size (9 pixels) in an YFP image. In each image, the averaged background intensity within 9 pixels was subtracted from the average fluorescence intensities of the neuronal regions. Intercellular calcium concentration change was estimated by taking the YFP/CFP fluorescence ratio (*Ratio*) and YFP/CFP ratio change from baseline (*Ratio change*), which was normalized within each assay (*Standardized ratio change*) to compare the activity among the assays. A median filter within a moving 15 sec temporal window was applied to the time course ratio to eliminate the noise independent from calcium signal. The image analysis for the immobilized condition was performed with ImageJ (NIH). Frames were aligned using the StackReg plugin. Intercellular calcium concentration change was estimated by taking the GCaMP/TagRFP fluorescence ratio (*Ratio*) and GCaMP/TagRFP ratio change from baseline (*Ratio change*), which was normalized within each recording (*Standardized ratio change*) to compare the activity among the recordings.

Quantification and Statistical Analysis. Experimental data are expressed as mean ± SEM. Simulation data are expressed as mean. For comparison of the data from behavioral analysis in MWT, we used a paired Student's *t*-test and a one-way ANOVA followed by a Tukey–Kramer post hoc multiple comparisons test. For comparison of the TTX indices, a Dunnett's multiple comparisons test was used to test the differences between wild-type animals and cell-ablated animals. For comparison of the data from imaging experiments, we used a Student's *t*-test and a paired Student's *t*-test. A difference is considered significant at a value of $^{**}P < 0.01$ or $^{*}P < 0.05$.

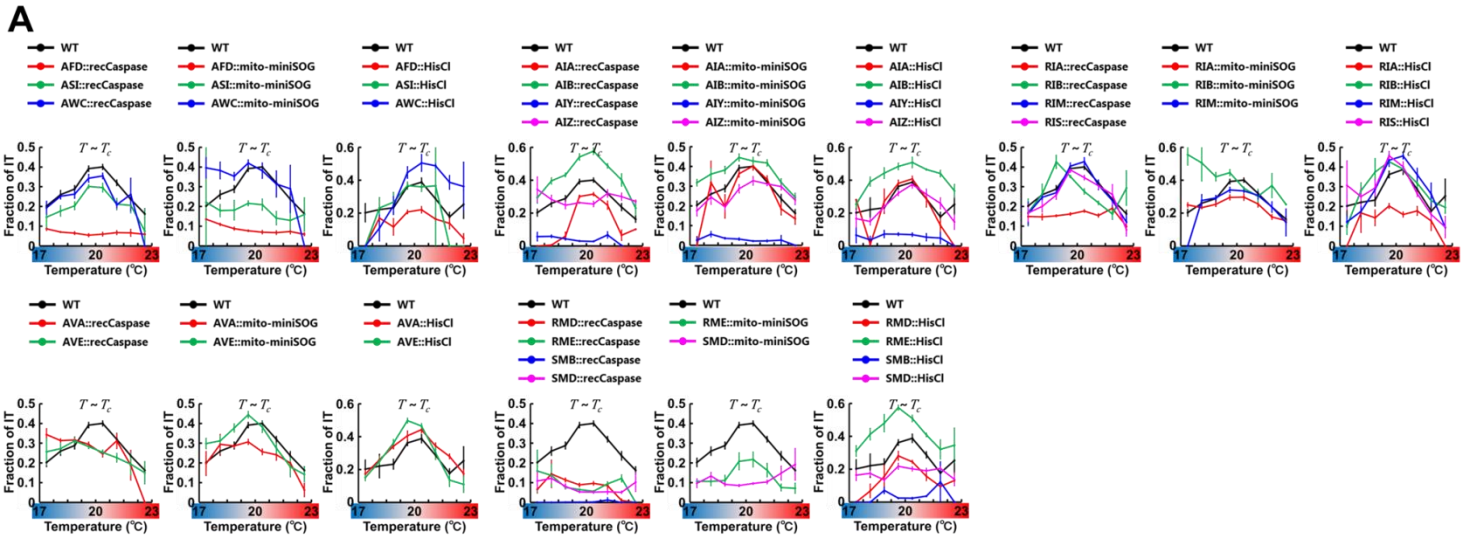
A
WT
AFD::recCaspase
ASI::recCaspase
AWC::recCaspase
AFD::mito-miniSOG
ASI::mito-miniSOG
AWC::mito-miniSOG
AFD::HisCl
ASI::HisCl
AWC::HisCl
AIA::recCaspase
AIB::recCaspase
AIY::recCaspase
AIZ::recCaspase
AIA::mito-miniSOG
AIB::mito-miniSOG
AIY::mito-miniSOG
AIZ::mito-miniSOG
AIA::HisCl
AIB::HisCl
AIY::HisCl
AIZ::HisCl
RIA::recCaspase
RIB::recCaspase
RIM::recCaspase
RIS::recCaspase
RIA::mito-miniSOG
RIB::mito-miniSOG
RIM::mito-miniSOG
RIA::HisCl
RIB::HisCl
RIM::HisCl
RIS::HisCl
AVA::recCaspase
AVE::recCaspase
AVA::mito-miniSOG
AVE::mito-miniSOG
AVA::HisCl
AVE::HisCl
RMD::recCaspase
RME::recCaspase
SMB::recCaspase
SMD::recCaspase
RME::mito-miniSOG
SMD::mito-miniSOG
RMD::HisCl
RME::HisCl
SMB::HisCl
SMD::HisCl
Fraction of IT
Temperature (℃)
T ~ Tc

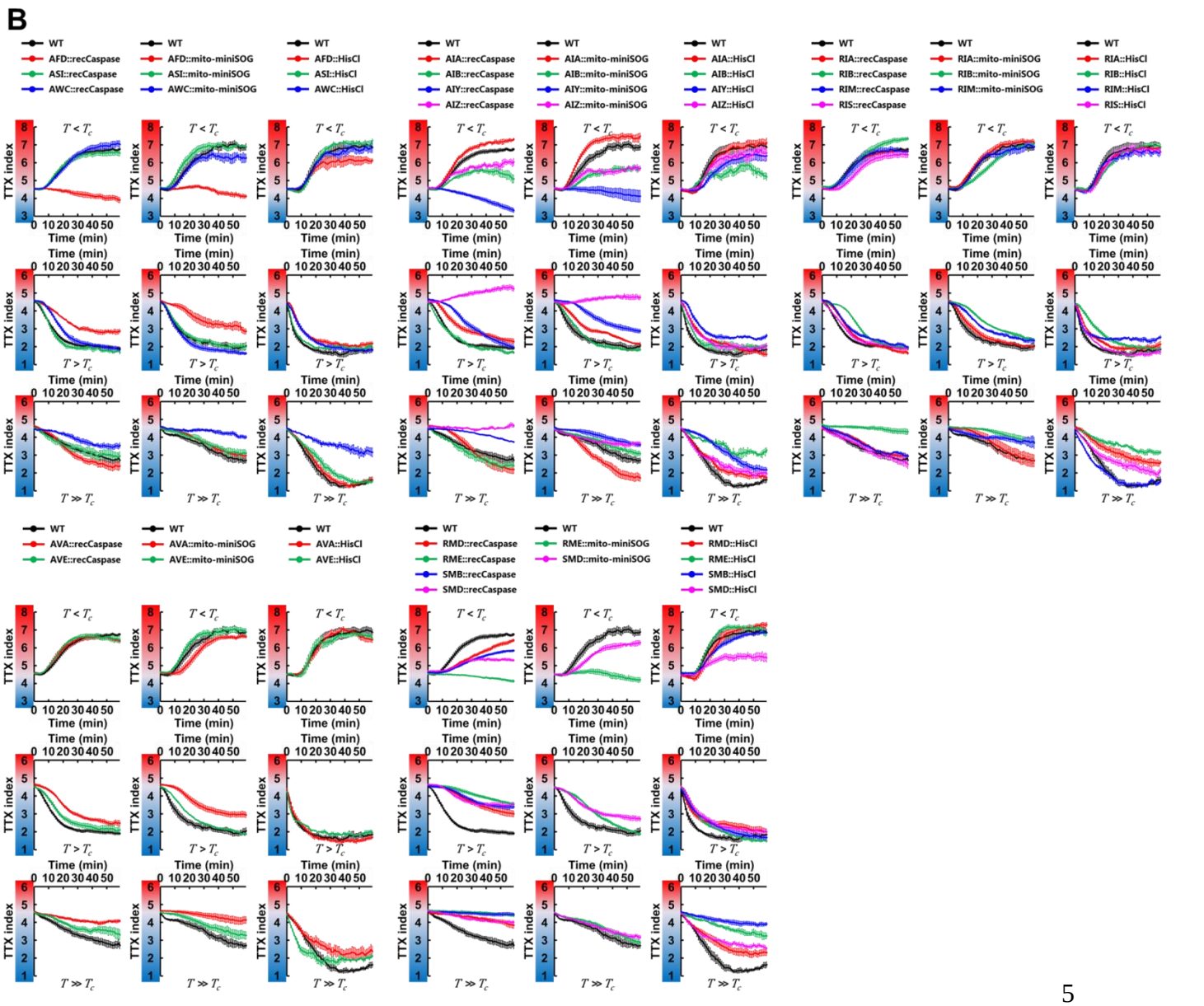
B
TTX index
Time (min)
T < Tc
T > Tc
T ≫ Tc

Fig. S1. Isothermal tracking and migration toward the T_c are executed by the distinct sets of neurons. (*A*) The fraction of IT as a function of the absolute temperature during 30–60 min after the start of the assays in the $T \sim T_c$ condition. (*B*) The time course of TTX indices in the $T < T_c$ condition (upper panels), in the $T > T_c$ condition (middle panels), and in the $T >> T_c$ condition (lower panels). Assays were performed under the deficiency of thermosensory neurons, amphid interneurons, ring interneurons, ventral cord interneurons, and ring motor neurons.

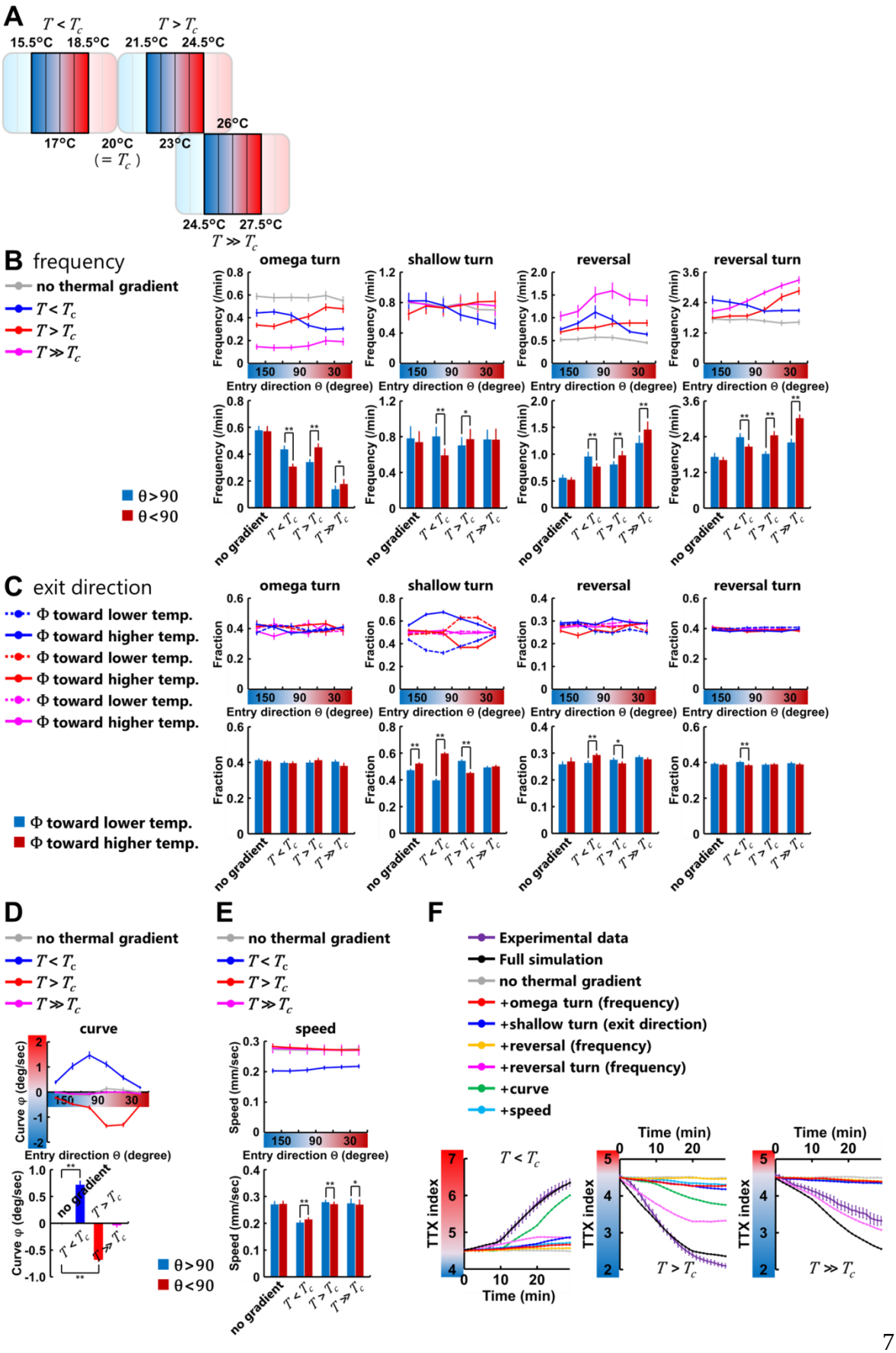
A
T < Tc
15.5°C
18.5°C
17°C
20°C
(= Tc)
T > Tc
21.5°C
24.5°C
23°C
26°C
24.5°C
27.5°C
T ≫ Tc
B frequency
no thermal gradient
T < Tc
T > Tc
T ≫ Tc
θ>90
θ<90
omega turn
shallow turn
reversal
reversal turn
Frequency (/min)
Entry direction θ (degree)
no gradient
C exit direction
Φ toward lower temp.
Φ toward higher temp.
Fraction
D
curve
Curve φ (deg/sec)
E
speed
Speed (mm/sec)
F
Experimental data
Full simulation
+omega turn (frequency)
+shallow turn (exit direction)
+reversal (frequency)
+reversal turn (frequency)
+curve
+speed
TTX index
Time (min)

Fig. S2. Behavioral components are employed differently depending on the distance of environmental temperature T to the T_c. (*A*) Temperature range within which the behavioral components were analyzed. Animals in the center four fractions of the assay plate were analyzed. (*B*) Upper right panels are frequency plots of the turns and the reversals representing the average as a function of the entry direction θ (left panel). Lower right panels show comparisons of the frequency of each behavioral event. Deep blue columns indicate the frequencies while the animals are moving down the thermal gradient (θ>90), and deep red columns the frequencies while moving up the thermal gradient (θ<90). (*C*) Fraction plots of the exit direction Φ after the turns and the reversals (left panel) representing the average as a function of the entry direction θ (upper right panel) and the averages in all the moving direction of animals (lower right panel). Dashed lines and deep blue columns indicate the fraction of Φ biased toward the lower temperature, and solid lines and deep red columns the fraction of Φ biased toward the higher temperature. (*D*) Plots of the biases φ of curves (left panel) representing the averages as a function of the entry direction θ (upper right panel) and the averages in all the moving direction of animals (lower right panel). φ is defined as positive if biased toward higher temperature and negative if biased toward lower temperature. (*E*) Upper panel is speed plots representing the averages as a function of the entry direction θ. Deep blue columns in lower panel indicate the speeds while the animals are moving down the thermal gradient (θ>90), and deep red columns the speeds while moving up the thermal gradient (θ<90). In (*B*–*E*), gray lines correspond to experiments without the thermal gradient (20°C constant), blue lines experiments in the $T<T_c$ condition, red lines experiments in the $T>T_c$ condition, and magenta lines experiments in the $T>>T_c$ condition (N = 9–12). The data of 20°C constant, in the $T<T_c$ condition, and in the $T>T_c$ condition are the same data set in Fig. 3. (*F*) The time course of TTX indices in the simulations and that obtained from experimental data (purple lines). Black lines correspond to the simulation in which all the data of wild-type animals determined by the experiment with the thermal gradient were used, and gray lines the simulation in which all the data of wild-type animals without the gradient were used. The other colored lines correspond to the simulation with the replacements of the individual behavioral components: the frequency of omega turns (red lines), the exit direction of shallow turns (blue lines), the frequency of reversals (yellow lines), the frequency of reversal turns (magenta lines), the curve (green lines), and the speed (light blue lines). The data in the $T<T_c$ and $T>T_c$ conditions are the same data set in Fig. 4. Error bars indicate SEM. (*B*,*C*,*E*) $^{**}P <$ 0.01 and $^{*}P < 0.05$ using paired Student's *t*-test; (*D*) $^{**}P < 0.01$ using one-way ANOVA followed by a Tukey–Kramer post hoc multiple comparisons test.

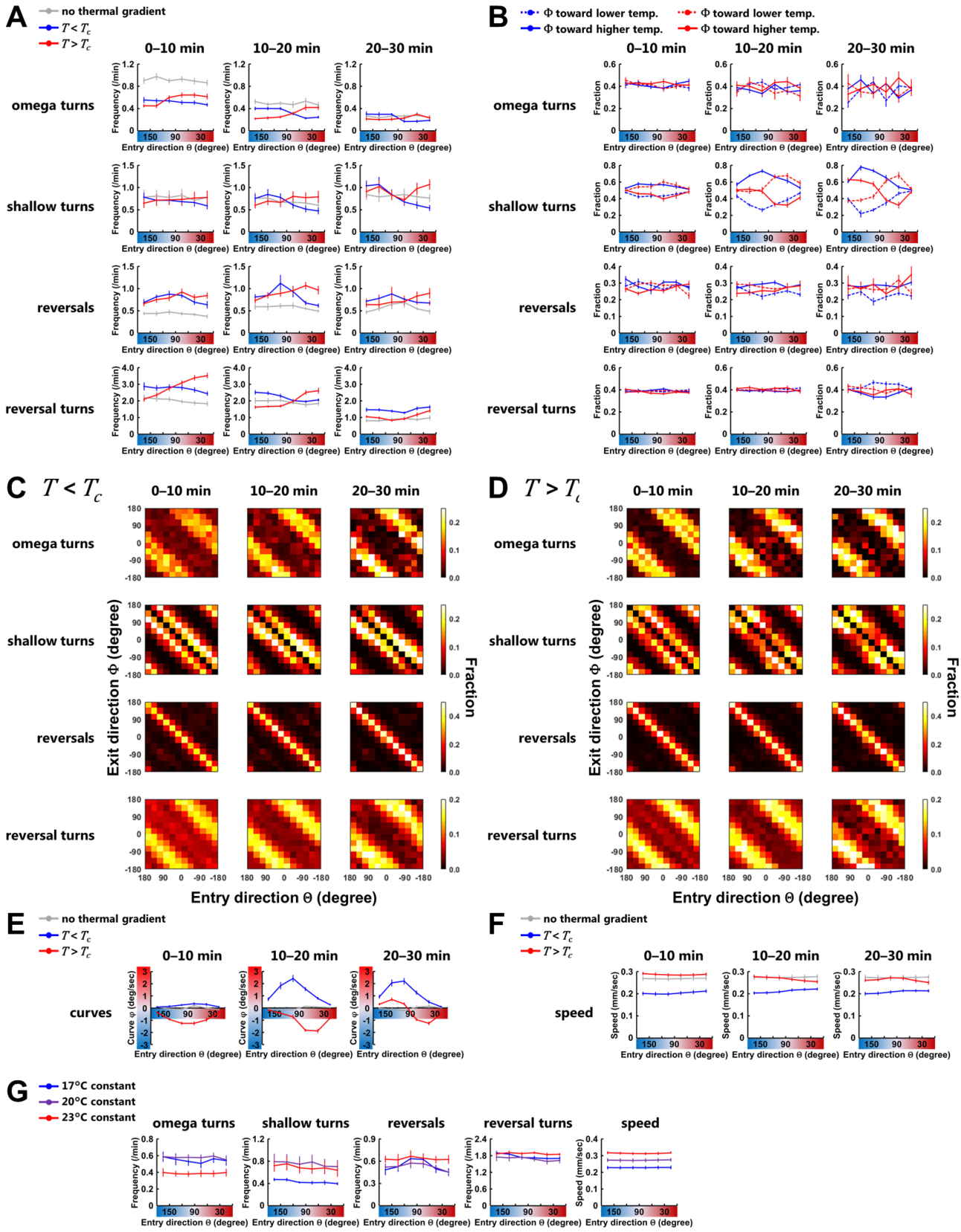
A
no thermal gradient
T < Tc
T > Tc
0–10 min
10–20 min
20–30 min
omega turns
shallow turns
reversals
reversal turns
Frequency (/min)
Entry direction Θ (degree)
B
Φ toward lower temp.
Φ toward higher temp.
Fraction
C
T < Tc
Exit direction Φ (degree)
Entry direction Θ (degree)
D
T > Tc
E
curves
Curve φ (deg/sec)
F
speed
Speed (mm/sec)
G
17°C constant
20°C constant
23°C constant

Fig. S3. Time course of the regulations of the behavioral components in wild-type animals. (*A*) Frequency plots of the turns and the reversals representing the averages as a function of the entry direction θ. Gray lines correspond to experiments without the thermal gradient (20°C constant), blue lines experiments in the $T<T_c$ condition, and red lines experiments in the $T>T_c$ condition. (*B*) Fraction plots of the exit direction Φ after the turns and the reversals representing the average as a function of the entry direction θ. Dashed lines indicate the exit directions of the events biased toward the lower temperature, and solid lines the exit directions biased toward the higher temperature. (*C* and *D*) Heatmaps of fraction of the exit direction Φ as functions of the entry direction θ in the $T<T_c$ condition (*C*) and in the $T>T_c$ condition (*D*). Both θ and Φ are signed to distinguish whether the exit angle is directed toward the upper half or the lower half of assay plates. (*E*) Plots of the biases φ of curves representing the averages as a function of the entry direction θ. (*F*) Speed plots representing the averages as a function of the entry direction θ. In (*E* and *F*), gray lines correspond to experiments without the thermal gradient (20°C constant), blue lines experiments in the $T<T_c$ condition, and red lines experiments in the $T>T_c$ condition. (*G*) Frequency plots of the turns and the reversals and speed plots representing the averages as a function of the entry direction θ on the constant temperature at 17°C (blue lines), 20°C (purple lines), and 23°C (red lines). In (*A*–*F*), the averages over 0–10 min (left columns), over 10–20 min (middle columns), and over 20–30 min (right columns) are shown. Error bars indicate SEM.

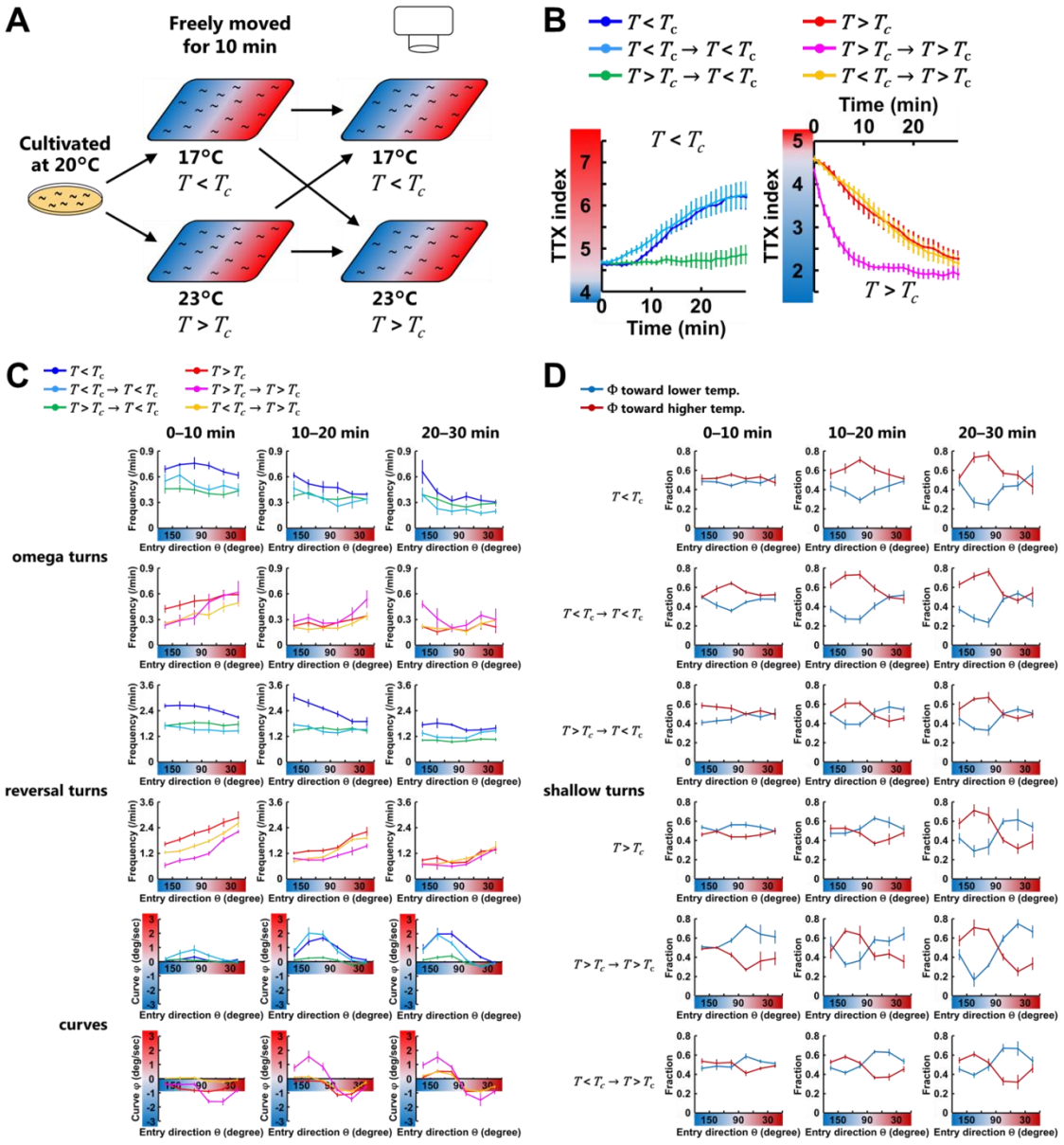

Fig. S4. Regulations of behavioral components are influenced by previous contexts. (*A*) Animals cultivated at 20°C were placed on a thermal gradient with 17°C or 23°C at the center for 10 min and then transferred on another thermal gradient with 17°C or 23°C at the center. (*B*) The time course of TTX indices after animals were transferred on the second plates (N = 4–6). (*C* and *D*) Time course of the regulations of the behavioral components. (*C*) Frequency plots of the omega turn (upper panels) and the reversal turn (middle panels) representing the averages as a function of the entry direction θ, and plots of the biases φ of curves representing the averages as a function of the entry direction θ (lower panels). In (*B* and *C*), blue lines correspond to experiments in the $T<T_c$ condition and red lines experiments in the $T>T_c$ condition. The other colored lines correspond to experiments accompanying the transfers of animals from the $T<T_c$ condition to the $T<T_c$ condition (cyan lines), from the $T>T_c$ condition to the $T<T_c$ condition (green lines), from the $T>T_c$ condition to the $T>T_c$ condition (magenta lines), and from the $T<T_c$ condition to the $T>T_c$ condition (yellow lines). (*D*) Fraction plots of the exit direction Φ after the shallow turns representing the averages as a function of the entry direction θ. Deep blue lines

indicate the exit directions of the events biased toward the lower temperature, and deep red lines the exit directions biased toward the higher temperature.

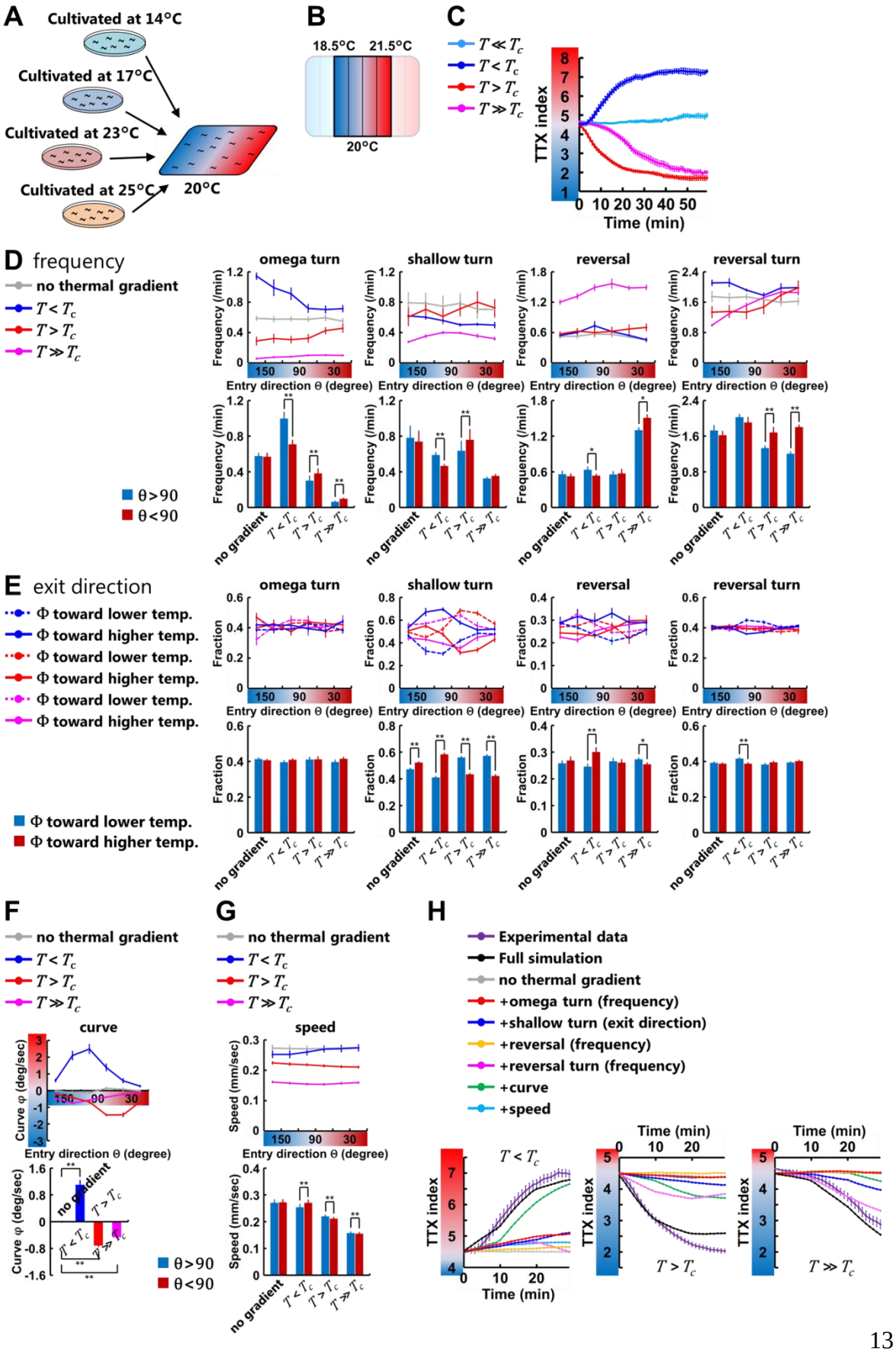
A
Cultivated at 14°C
Cultivated at 17°C
Cultivated at 23°C
Cultivated at 25°C
20°C
B
18.5°C
21.5°C
20°C
C
$T \ll T_c$
$T < T_c$
$T > T_c$
$T \gg T_c$
TTX index
Time (min)
D frequency
no thermal gradient
$T < T_c$
$T > T_c$
$T \gg T_c$
θ>90
θ<90
omega turn
shallow turn
reversal
reversal turn
Frequency (/min)
Entry direction θ (degree)
no gradient
E exit direction
Φ toward lower temp.
Φ toward higher temp.
Fraction
F
curve
Curve φ (deg/sec)
G
speed
Speed (mm/sec)
H
Experimental data
Full simulation
no thermal gradient
+omega turn (frequency)
+shallow turn (exit direction)
+reversal (frequency)
+reversal turn (frequency)
+curve
+speed

Fig. S5. Behavioral components are employed differently depending on the environmental temperature T relative to the T_c. (*A*) Animals cultivated at 14°C ($T>>T_c$), 17°C ($T>T_c$), 23°C ($T<T_c$), or 25°C ($T<<T_c$) were placed on a thermal gradient with 20°C at the center. The plate was maintained with a linear thermal gradient of approximately 0.45 °C/cm. (*B*) Temperature range within which the behavioral components were analyzed. Animals in the center four fractions of the assay plate were analyzed. (*C*) The time course of TTX indices in the $T<<T_c$ condition (cyan line), in the $T<T_c$ condition (blue line), in the $T>T_c$ condition (red line), and in the $T>>T_c$ condition (red line) (N = 6). (*D*) Upper panels are frequency plots of the turns and the reversals representing the averages as a function of the entry direction θ. Lower panels show comparisons of the frequency of each behavioral event. Deep blue columns indicate the frequencies of the events while the animals are moving down the thermal gradient (θ>90), and deep red columns the frequencies while moving up the thermal gradient (θ<90). (*E*) Upper panels are fraction plots of the exit direction Φ after the turns and the reversals representing the average as a function of the entry direction θ. Deep blue lines indicate the exit directions of the events biased toward the lower temperature, and deep red lines the exit directions biased toward the higher temperature. Bottom panels show comparisons of the fraction of the exit direction of each behavioral event. Deep blue columns indicate the exit directions of the events biased toward the lower temperature, and deep red columns the exit directions biased toward the higher temperature. (*F*) Plots of the biases φ of curves representing the averages as a function of the entry direction θ (upper panel) and the averages in all the moving direction of animals (lower panel). (*G*) Upper panel is speed plots representing the averages as a function of the entry direction θ. Lower panel shows comparisons of the speeds. Deep blue columns indicate the speeds while the animals are moving down the thermal gradient (θ>90), and deep red columns the speeds while moving up the thermal gradient (θ<90). In (*D–G*), gray lines correspond to experiments without the thermal gradient (20°C constant), blue lines experiments in the $T<T_c$ condition, red lines experiments in the $T>T_c$ condition, and magenta lines experiments in the $T>>T_c$ condition. The data of 20°C constant are the same data set in Fig. 3. (*H*) The time course of TTX indices in the simulations and that obtained from experimental data (purple lines). Black lines correspond to the simulation in which all the data of wild-type animals determined by the experiment with the thermal gradient were used, and gray lines the simulation in which all the data of wild-type animals without the gradient were used. The other colored lines correspond to the simulation with the replacements of the individual behavioral components: the frequency of omega turns (red lines), the exit direction of shallow turns (blue lines), the frequency of reversals (yellow lines), the frequency of reversal turns (magenta lines), the curve (green lines), and the speed (light blue lines). Error bars indicate SEM. (*D,E,G*) $^{**}P < 0.01$ and $^{*}P < 0.05$ using paired Student's *t*-test; (*F*) $^{**}P < 0.01$ using one-way ANOVA followed by a Tukey–Kramer post hoc multiple comparisons test.

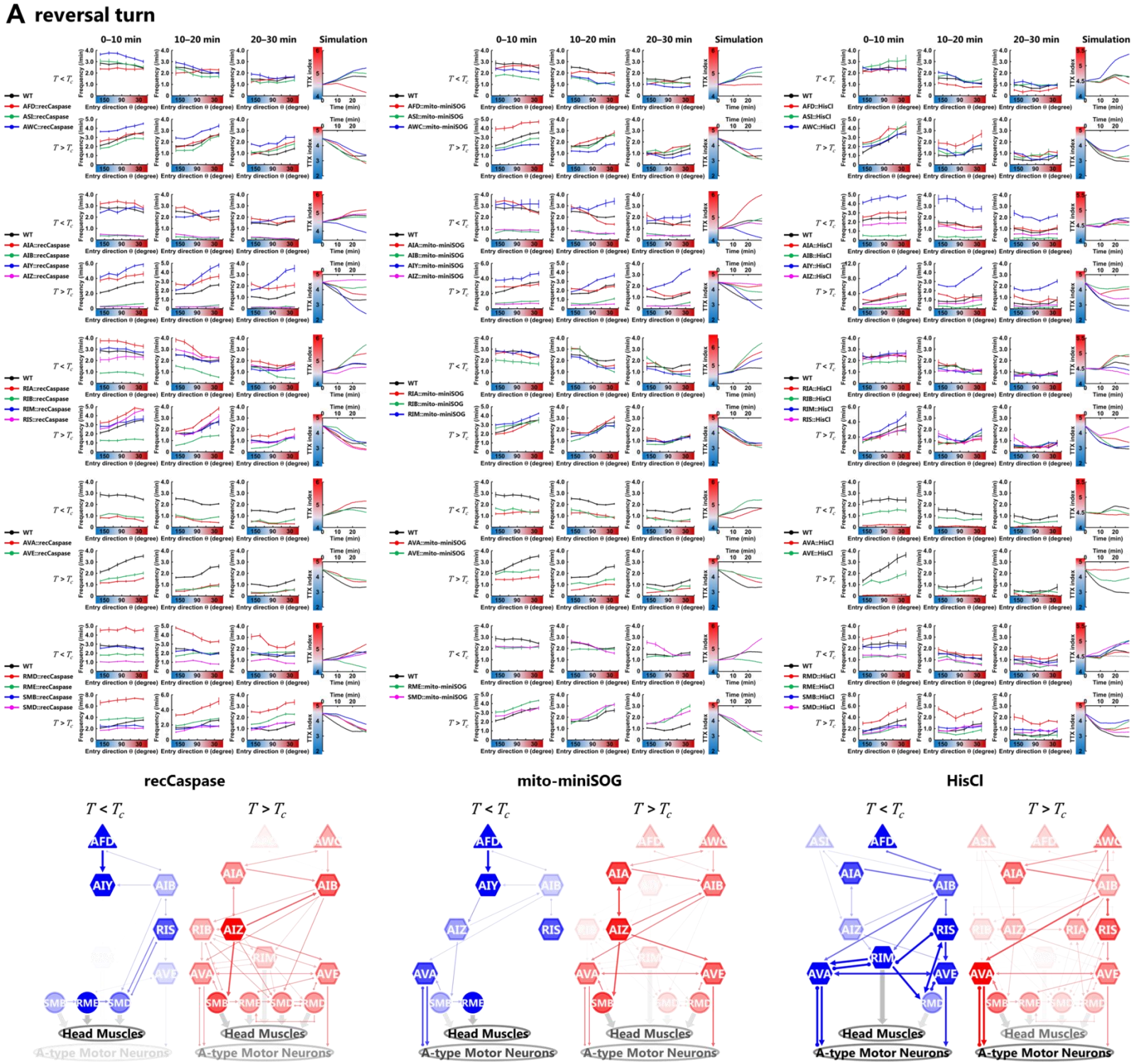
A reversal turn
0–10 min
10–20 min
20–30 min
Simulation
T < Tc
T > Tc
Frequency (/min)
Entry direction θ (degree)
TTX index
Time (min)
WT
AFD::recCaspase
ASI::recCaspase
AWC::recCaspase
AIA::recCaspase
AIB::recCaspase
AIY::recCaspase
AIZ::recCaspase
RIA::recCaspase
RIB::recCaspase
RIM::recCaspase
RIS::recCaspase
AVA::recCaspase
AVE::recCaspase
RMD::recCaspase
RME::recCaspase
SMB::recCaspase
SMD::recCaspase
AFD::mito-miniSOG
ASI::mito-miniSOG
AWC::mito-miniSOG
AIA::mito-miniSOG
AIB::mito-miniSOG
AIY::mito-miniSOG
AIZ::mito-miniSOG
RIA::mito-miniSOG
RIB::mito-miniSOG
RIM::mito-miniSOG
AVA::mito-miniSOG
AVE::mito-miniSOG
RME::mito-miniSOG
SMD::mito-miniSOG
AFD::HisCl
ASI::HisCl
AWC::HisCl
AIA::HisCl
AIB::HisCl
AIY::HisCl
AIZ::HisCl
RIA::HisCl
RIB::HisCl
RIM::HisCl
RIS::HisCl
AVA::HisCl
AVE::HisCl
RMD::HisCl
RME::HisCl
SMB::HisCl
SMD::HisCl
recCaspase
mito-miniSOG
HisCl
T < Tc
T > Tc
AFD
AWC
AIA
AIB
AIY
AIZ
RIS
RIB
RIM
AVA
AVE
SMB
RME
SMD
RMD
Head Muscles
A-type Motor Neurons

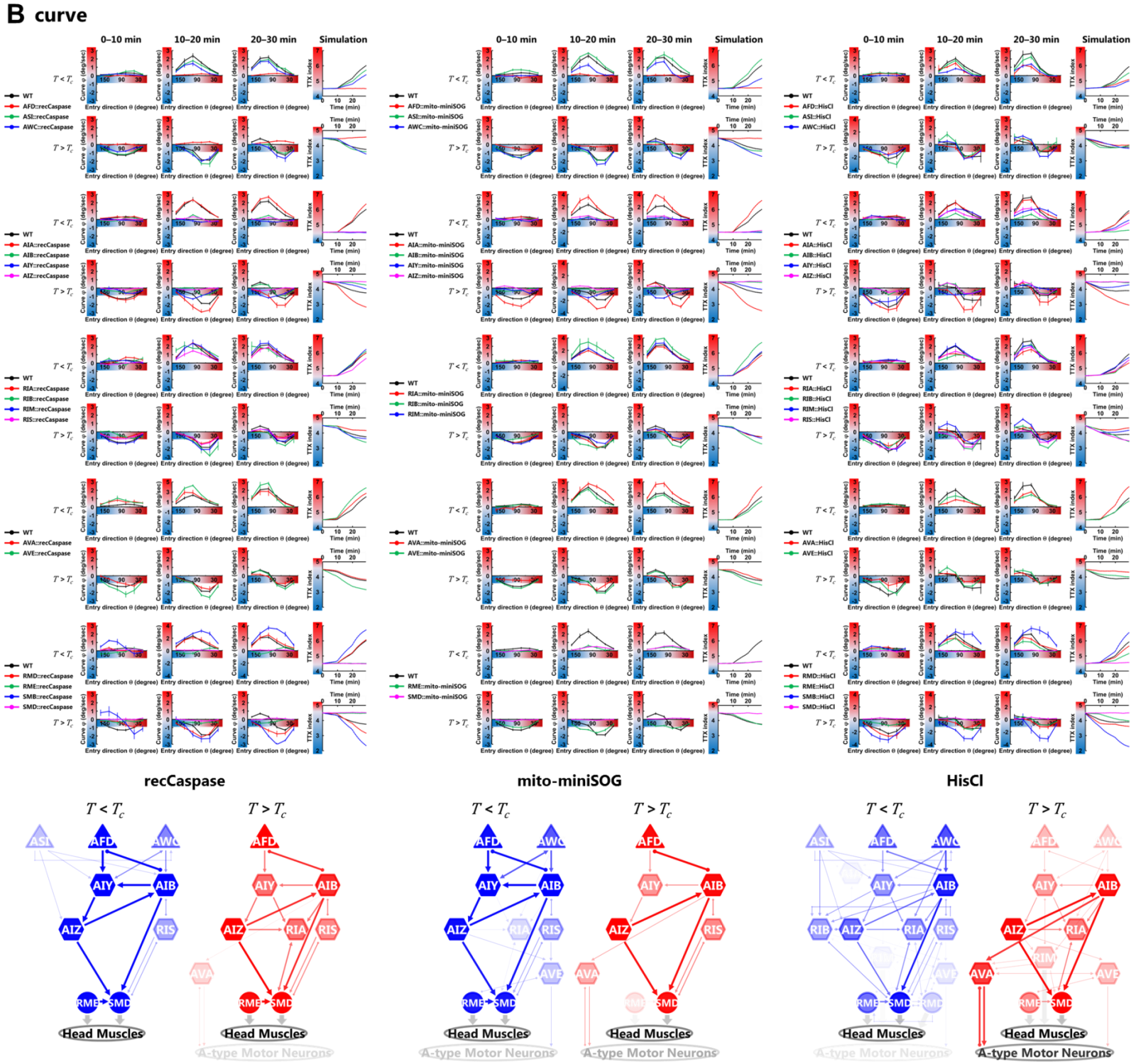
B curve
0–10 min
10–20 min
20–30 min
Simulation
recCaspase
mito-miniSOG
HisCl
Head Muscles
A-type Motor Neurons

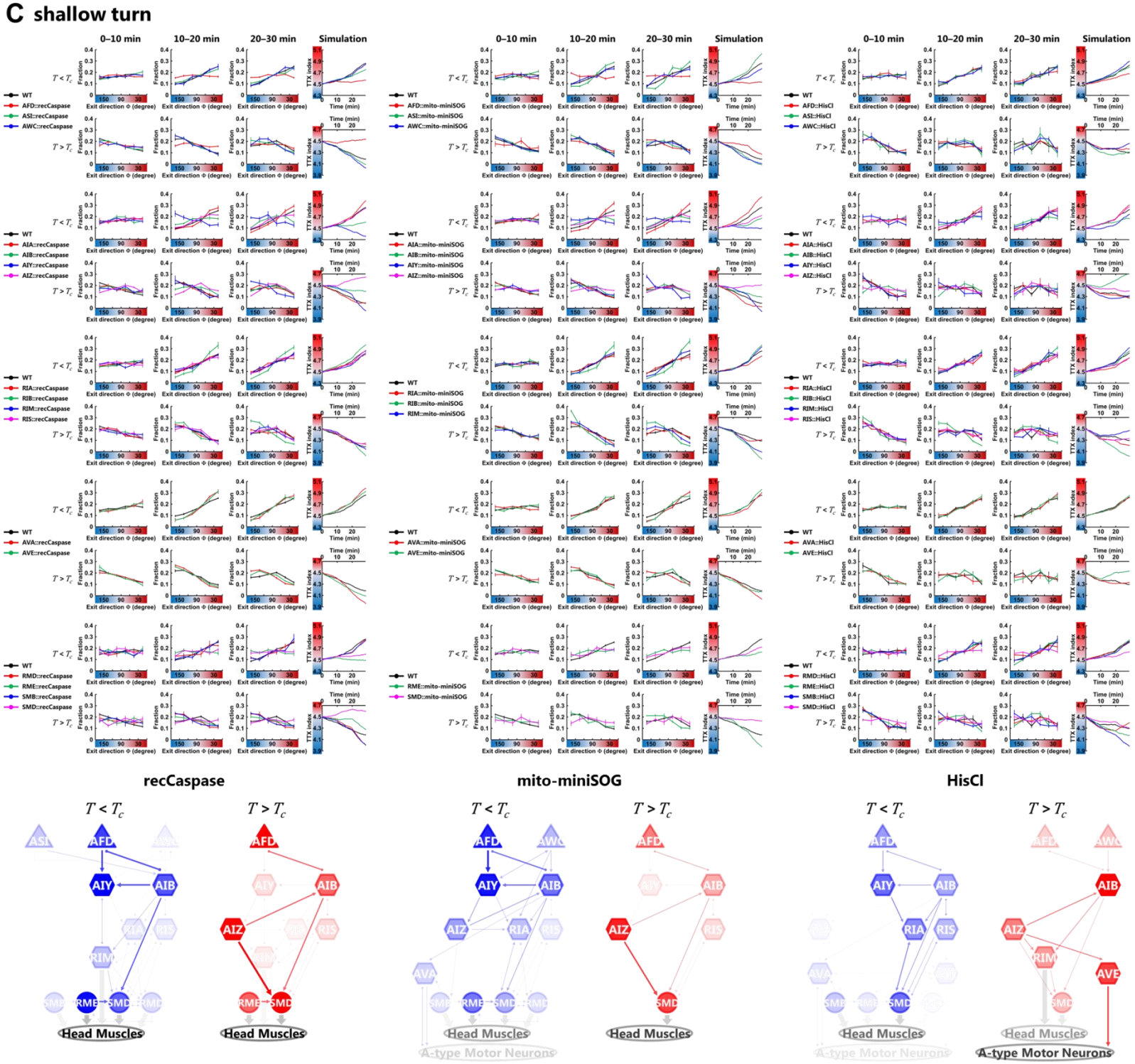
C shallow turn
0–10 min
10–20 min
20–30 min
Simulation
T < Tc
T > Tc
Fraction
Exit direction Φ (degree)
TTX index
Time (min)
WT
AFD::recCaspase
ASI::recCaspase
AWC::recCaspase
AFD::mito-miniSOG
ASI::mito-miniSOG
AWC::mito-miniSOG
AFD::HisCl
ASI::HisCl
AWC::HisCl
AIA::recCaspase
AIB::recCaspase
AIY::recCaspase
AIZ::recCaspase
AIA::mito-miniSOG
AIB::mito-miniSOG
AIY::mito-miniSOG
AIZ::mito-miniSOG
AIA::HisCl
AIB::HisCl
AIY::HisCl
AIZ::HisCl
RIA::recCaspase
RIB::recCaspase
RIM::recCaspase
RIS::recCaspase
RIA::mito-miniSOG
RIB::mito-miniSOG
RIM::mito-miniSOG
RIA::HisCl
RIB::HisCl
RIM::HisCl
RIS::HisCl
AVA::recCaspase
AVE::recCaspase
AVA::mito-miniSOG
AVE::mito-miniSOG
AVA::HisCl
AVE::HisCl
RMD::recCaspase
RME::recCaspase
SMB::recCaspase
SMD::recCaspase
RME::mito-miniSOG
SMD::mito-miniSOG
RMD::HisCl
RME::HisCl
SMB::HisCl
SMD::HisCl
recCaspase
mito-miniSOG
HisCl
T < Tc
T > Tc
ASI
AFD
AWC
AIY
AIB
AIZ
RIA
RIS
RIM
AVA
AVE
RME
SMD
Head Muscles
A-type Motor Neurons


D omega turn
0–10 min
10–20 min
20–30 min
Simulation
T < Tc
T > Tc
Frequency (/min)
Entry direction θ (degree)
TTX index
Time (min)
WT
AFD::recCaspase
ASI::recCaspase
AWC::recCaspase
AFD::mito-miniSOG
ASI::mito-miniSOG
AWC::mito-miniSOG
AFD::HisCl
ASI::HisCl
AWC::HisCl
AIA::recCaspase
AIB::recCaspase
AIY::recCaspase
AIZ::recCaspase
AIA::mito-miniSOG
AIB::mito-miniSOG
AIY::mito-miniSOG
AIZ::mito-miniSOG
AIA::HisCl
AIB::HisCl
AIY::HisCl
AIZ::HisCl
RIA::recCaspase
RIB::recCaspase
RIM::recCaspase
RIS::recCaspase
RIA::mito-miniSOG
RIB::mito-miniSOG
RIM::mito-miniSOG
RIA::HisCl
RIB::HisCl
RIM::HisCl
RIS::HisCl
AVA::recCaspase
AVE::recCaspase
AVA::mito-miniSOG
AVE::mito-miniSOG
AVA::HisCl
AVE::HisCl
RMD::recCaspase
RME::recCaspase
SMB::recCaspase
SMD::recCaspase
RME::mito-miniSOG
SMD::mito-miniSOG
RMD::HisCl
RME::HisCl
SMB::HisCl
SMD::HisCl
recCaspase
mito-miniSOG
HisCl
T < Tc
T > Tc
AFD
AIY
AIZ
RME
SMD
Head Muscles
AWC
AIA
AIB
RIA
RIS
RIB
RIM
AVA
AVE
RMD
A-type Motor Neurons
ASI


E speed
0–10 min
10–20 min
20–30 min
Simulation
T < Tc
T > Tc
Speed (mm/sec)
Entry direction θ (degree)
TTX index
Time (min)
WT
AFD::recCaspase
ASI::recCaspase
AWC::recCaspase
AFD::mito-miniSOG
ASI::mito-miniSOG
AWC::mito-miniSOG
AFD::HisCl
ASI::HisCl
AWC::HisCl
AIA::recCaspase
AIB::recCaspase
AIY::recCaspase
AIZ::recCaspase
AIA::mito-miniSOG
AIB::mito-miniSOG
AIY::mito-miniSOG
AIZ::mito-miniSOG
AIA::HisCl
AIB::HisCl
AIY::HisCl
AIZ::HisCl
RIA::recCaspase
RIB::recCaspase
RIM::recCaspase
RIS::recCaspase
RIA::mito-miniSOG
RIB::mito-miniSOG
RIM::mito-miniSOG
RIA::HisCl
RIB::HisCl
RIM::HisCl
RIS::HisCl
AVA::recCaspase
AVE::recCaspase
AVA::mito-miniSOG
AVE::mito-miniSOG
AVA::HisCl
AVE::HisCl
RMD::recCaspase
RME::recCaspase
SMB::recCaspase
SMD::recCaspase
RME::mito-miniSOG
SMD::mito-miniSOG
RMD::HisCl
RME::HisCl
SMB::HisCl
SMD::HisCl
recCaspase
mito-miniSOG
HisCl
ASI
AFD
AWC
AIA
AIB
AIY
RIB
AIZ
RIS
AVA
AVE
SMB
RME
SMD
RMD
Head Muscles
A-type Motor Neurons

Fig. S6. Time course of the regulations of the behavioral components in cell-ablated/silenced animals. Upper panels are plots of the frequency of reversal turns (*A*), the bias φ of curves (*B*), the exit direction Φ after shallow turns (*C*), the frequency of omega turns (*D*), and the speeds (*E*) representing the averages as a function of the entry direction θ. The averages over 0–10 min (first columns), over 10–20 min (second columns), over 20–30 min (third columns), and the time course of TTX indices in the simulations (fourth columns) are shown (N = 4–12). Lower panels are neural diagrams for mediating the biases in the individual behavioral components in the $T<T_c$ condition (blue) and in the $T>T_c$ condition (red). The thickness and color strength of each neuron represent the functional importance of the neuron predicted from the analysis and were determined as follows: For each neuron, the differences between the migration index of the wild-type animals and the index of the cell-ablated/silenced animals expressing reconstituted caspases (left panels), mito-miniSOG (middle panels), or HisCl1 (right panels) were calculated. The difference is used to determine the color strength, where the color strength of each neuron is proportional to this value. The color strength of each line is identical to the strength of the color of one of the two connected neurons with lower strength, and the thickness of each line is proportional to this color strength. In RIS, SMB, and RMD neurons in the middle diagram, we applied the data of the animals expressing recCaspase because we could not obtain the animals expressing mito-miniSOG specifically in these neurons. The right diagram for reversal turns in the $T<T_c$ condition was determined by the data in 10–30 min because we observed unexpected bias that drives sims away from T_c in 0–10 min. The right diagram for speeds in the $T>T_c$ condition was determined by the data in 0–10 min because we observed unexpected bias that drives sims away from T_c in 10–30 min.

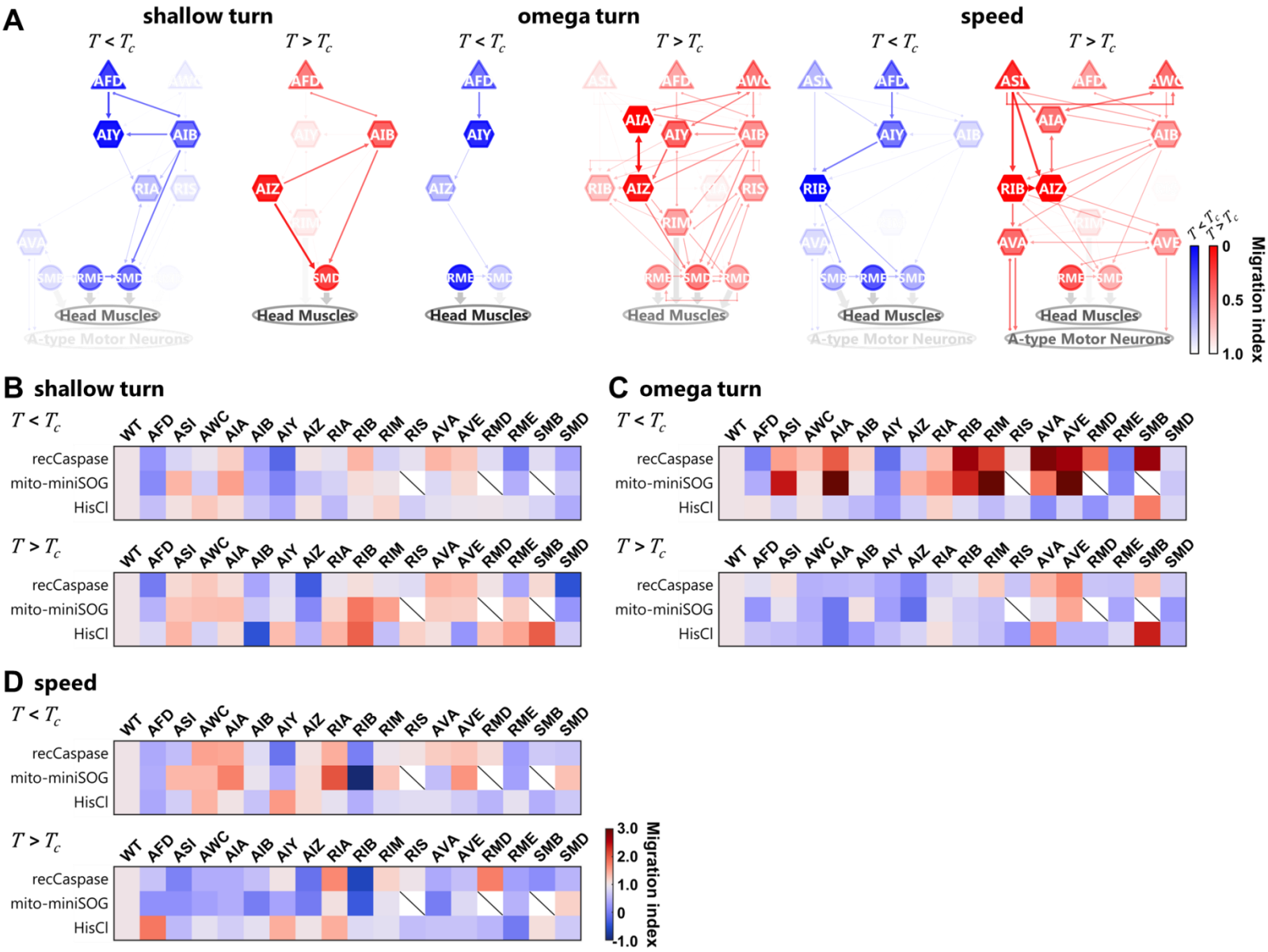

Fig. S7. Distinct sets of neurons are responsible for the context-dependent biases in the behavioral components. (*A*) Neural diagrams responsible for generating the biases in the shallow turns, the omega turns, and the speeds in the $T<T_c$ condition (blue) and in the $T>T_c$ condition (red). The thickness and color strength of each neuron represent the functional importance of the neuron predicted from the analysis and were determined as follows: For each neuron, the differences between the migration index of the wild-type animals and the index of the cell-ablated/silenced animals expressing reconstituted caspases, mito-miniSOG, or HisCl1 were calculated. The median difference from the three ablation strategies (or the smaller difference from the two strategies) is used to determine the color strength, where the color strength of each neuron is proportional to this value. The color strength of each line is identical to the strength of the color of one of the two connected neurons with lower strength, and the thickness of each line is proportional to this color strength. (*B–D*) Heatmaps showing migration indices of the shallow turns (*B*), the omega turns (*C*), and the speeds (*D*) after cell-specific ablation and silencing in the $T<T_c$ condition (upper panels) and in the $T>T_c$ condition (lower panels).

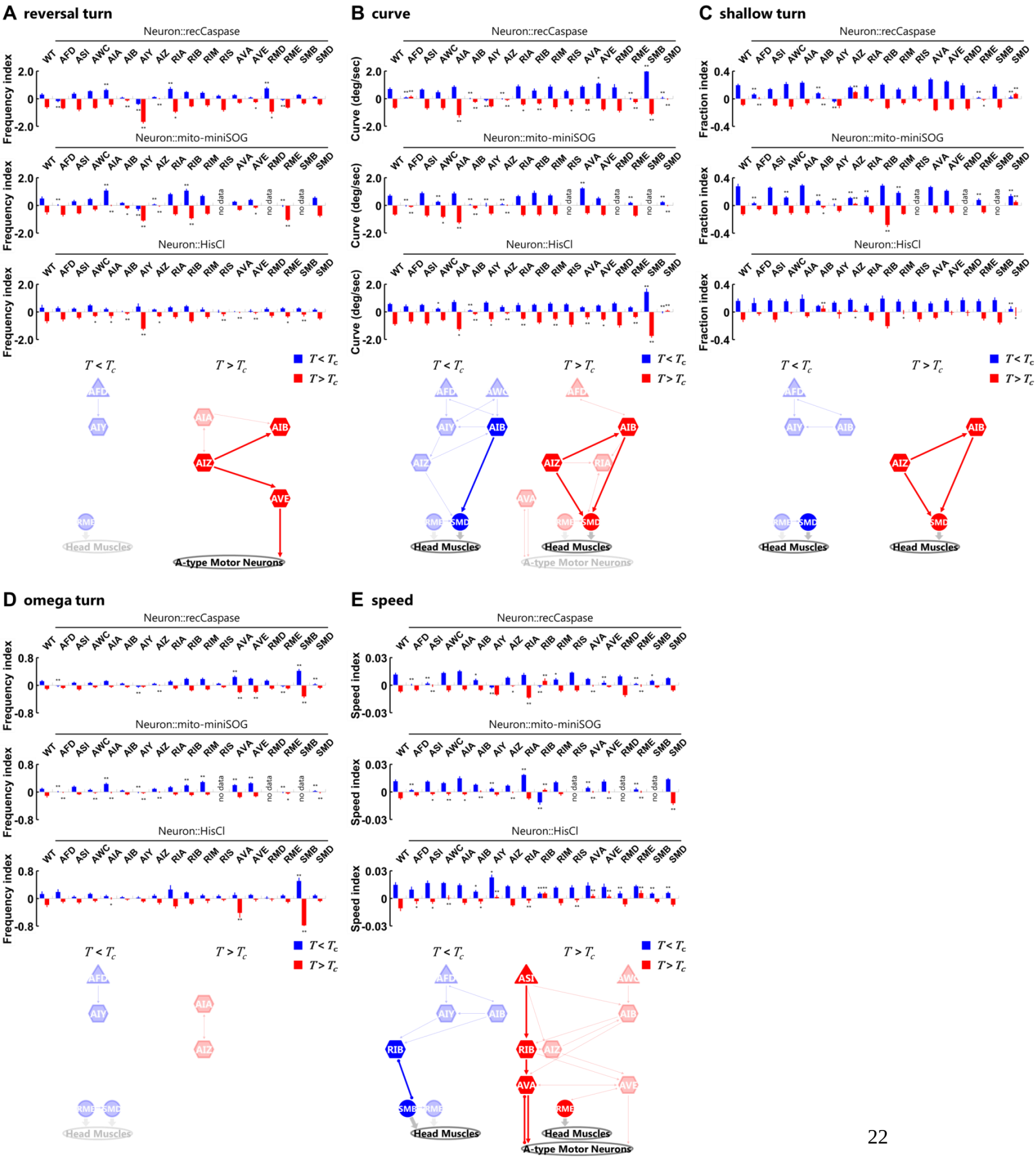
A reversal turn
B curve
C shallow turn
D omega turn
E speed
Neuron::recCaspase
Neuron::mito-miniSOG
Neuron::HisCl
Frequency index
Curve (deg/sec)
Fraction index
Speed index
WT AFD ASI AWC AIA AIB AIY AIZ RIA RIB RIM RIS AVA AVE RMD RME SMB SMD
no data
T < Tc
T > Tc
AFD
AWC
AIY
AIA
AIB
AIZ
RIA
AVE
AVA
ASI
RIB
RME
SMD
SMB
Head Muscles
A-type Motor Neurons

Fig. S8. Comparisons of the biases in the behavioral components of cell-ablated/silenced animals. Following the previous study (11), we compared the biases in the reversal turns (*A*), the curves (*B*), the shallow turns (*C*), the omega turns (*D*), and the speeds (*E*). Frequency index was defined as the difference between the frequencies of the events while the animals are moving down the thermal gradient and while moving up the gradient. Biases of the curves were compared by averaging curves in all the moving direction of animals. Fraction index was defined as the difference between the exit directions of the events biased toward the higher temperature and toward the lower temperature. Speed index was defined as the difference between the speeds while the animals are moving up the thermal gradient and while moving down the gradient. In (*A*–*E*), blue columns indicate the indices or the biases in the $T<T_c$ condition and red columns the indices or the biases in the $T>T_c$ condition. In below panels, the neurons in which their removal showed significant impairment of the indices or the biases in all the genetic manipulations are shown in deep color, and the neurons in which their removal showed significant impairment in at least two of three manipulations are shown in pale color. Error bars indicate SEM. $^{**}P < 0.01$ and $^{*}P < 0.05$, different from WT, using Dunnett's multiple comparisons test.

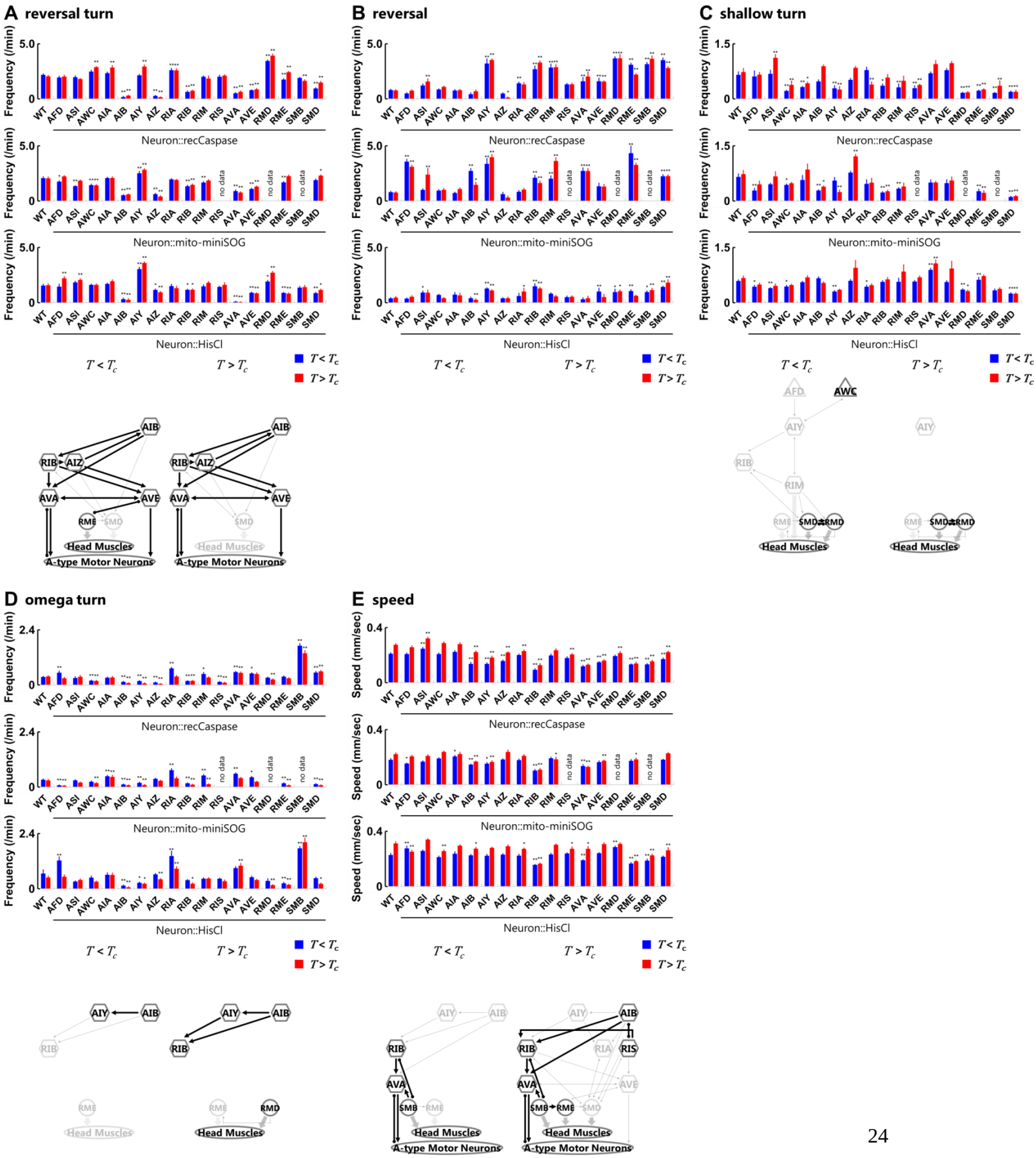
A reversal turn
B reversal
C shallow turn
D omega turn
E speed
Frequency (/min)
Speed (mm/sec)
Neuron::recCaspase
Neuron::mito-miniSOG
Neuron::HisCl
WT AFD ASI AWC AIA AIB AIY AIZ RIA RIB RIM RIS AVA AVE RMD RME SMB SMD
no data
T < Tc
T > Tc
AIB
RIB
AIZ
AVA
AVE
RME
SMD
Head Muscles
A-type Motor Neurons
AFD
AWC
AIY
RIM
RMD
RIA
RIS

Fig. S9. Comparisons of the basal levels of the behavioral components in cell-ablated/silenced animals. Blue columns indicate the frequencies of reversal turns (*A*), reversals (*B*), shallow turns (*C*), omega turns (*D*), and the speeds (*E*) in the $T<T_c$ condition, and red columns the speeds and the frequencies in the $T>T_c$ condition. Basal levels were determined by averaging the turning frequencies and the speeds in all the moving direction of animals. In below panels, the neurons in which their removal showed significant impairment of the frequencies or the speeds in all the genetic manipulations are shown in deep color, and the neurons in which their removal showed significant impairment in at least two of three manipulations are shown in pale color. Error bars indicate SEM. $^{**}P < 0.01$ and $^{*}P < 0.05$, different from WT, using Dunnett's multiple comparisons test.

Table S1. Cell-ablated strains used in this study. Efficiencies of cell-ablations by recCaspasese were estimated by crossing the listed lines into integrated reporter lines listed in *SI Appendix*, Table S3 and scoring the disappearance of fluorescence from the reporter proteins. *Efficiency of *njIs93* was estimated in the heterozygous state. Efficiencies of cell-ablations by mito-miniSOG were estimaterd by scoring the disappearance of fluorescence from the miniSOG after the illumination of blue light at the L1 stage.

Strain name	Genotype	Experiment	Ablation Efficiency (%)
IK2809	*njIs80[gcy-8p::cz::caspase-3(p17), gcy-8p::caspase-3(p12)::nz, ges-1p::nls-GFP] (X)*	AFD ablation	100
IK3048	*njIs89[gcy-8p::tomm-20(N'-55AA)::miniSOG, ges-1p::nls-GFP] (III)*		92.7
PY7505	*oyIs84[gcy-27p::cz::caspase-3(p17), gpa-4p::caspase-3(p12)::nz, gcy-27p::GFP, unc-122p::dsRed]*	ASI ablation	(Beverly et al., 2011)
IK3176	*njIs104[gpa-4p::flp, gcy-27p::frt::tomm-20(N'-55AA)::miniSOG, ges-1p::nls-GFP] (IV)*		91.9
IK2808	*njIs79[ceh-36p::cz::caspase-3(p17), ceh-36p::caspase-3(p12)::nz, ges-1p::nls-GFP] (X)*	AWC ablation	98.4
IK3125	*njIs98[ceh-36p::tomm-20(N'-55AA)::miniSOG, ges-1p::nls-GFP] (I)*		100
IK3263	*njIs120[ins-1p::cz::caspase-3(p17), gcy-28dp::caspase-3(p12)::nz, ges-1p::nls-GFP] (V)*	AIA ablation	64.6
IK3240	*njIs115[ins-1p::flp, gcy-28dp::frt::tomm-20(N'-55AA)::miniSOG, ges-1p::nls-GFP] (IV)*		74.1
IK3449	*njIs133[aptf-1p::cz::caspase-3(p17), inx-1p::caspase-3(p12)::nz, ges-1p::nls-GFP] (II)*	AIB ablation	87.4
IK3388	*njIs131[odr-2(2b)p::flp, inx-1p::frt::tomm-20(N'-55AA)::miniSOG, ges-1p::nls-GFP] (X)*		100
IK2710	*njIs62[AIYp::cz::caspase-3(p17), AIYp::caspase-3(p12)::nz, ges-1p::nls-GFP] (V)*	AIY ablation	100
IK2962	*njIs87[AIYp::tomm-20(N'-55AA)::miniSOG, ges-1p::nls-GFP] (IV)*		100
IK3179	*njIs107[acc-2p::cz::caspase-3(p17), odr-2(2b)p::caspase-3(p12)::nz, ges-1p::nls-GFP] (IV)*	AIZ ablation	100
IK3241	*njIs116[acc-2p::flp, odr-2(2b)p::frt::tomm-20(N'-55AA)::miniSOG, ges-1p::nls-GFP] (IV)*		99.7
IK2910	*njIs84[glr-3p::cz::caspase-3(p17), glr-3p::caspase-3(p12)::nz, ges-1p::nls-GFP] (III)*	RIA ablation	100
IK3289	*njIs123[glr-3p::tomm-20(N'-55AA)::miniSOG, ges-1p::nls-GFP] (V)*		100
IK3049	*njIs90[trp-1p::cz::caspase-3(p17), sto-3p::caspase-3(p12)::nz, ges-1p::nls-GFP] (I)*	RIB ablation	96.6
IK3238	*njIs113[ser-4p::flp, sto-3p::frt::tomm-20(N'-55AA)::miniSOG, ges-1p::nls-GFP] (II)*		95.5
IK3067	*njIs93[glr-1p::cz::caspase-3(p17), tdc-1p::caspase-3(p12)::nz, ges-1p::nls-GFP] (X)*	RIM ablation	66.7*
IK3144	*njIs100[glr-1p::flp, tdc-1p::frt::tomm-20(N'-55AA)::miniSOG, ges-1p::nls-GFP] (III)*		92.9
IK3325	*njIs126[nlr-1p::cz::caspase-3(p17), ggr-2p::caspase-3(p12)::nz, ges-1p::nls-GFP] (V)*	RIS ablation	98.5
IK3175	*njIs103[nmr-1p::cz::caspase-3(p17), flp-18p::caspase-3(p12)::nz, ges-1p::nls-GFP] (II)*	AVA ablation	100
IK3327	*njIs128[flp-18p::flp, nmr-1p::frt::tomm-20(N'-55AA)::miniSOG, ges-1p::nls-GFP] (II)*		82.7
IK3177	*njIs105[nmr-1p::cz::caspase-3(p17), opt-3p::caspase-3(p12)::nz, ges-1p::nls-GFP] (X)*	AVE ablation	97.8
IK3324	*njIs125[opt-3p::flp, nmr-1p::frt::tomm-20(N'-55AA)::miniSOG, ges-1p::nls-GFP] (X)*		100
IK3237	*njIs121[glr-1p::cz::caspase-3(p17), mgl-1p::caspase-3(p12)::nz, ges-1p::nls-GFP] (II)*	RMD/D/V ablation	34.8
IK3404	*njIs132[ser-2(2)p::cz::caspase-3(p17), ntr-2p::caspase-3(p12)::nz, ges-1p::nls-GFP] (X)*	RMED/V ablation	56.9
IK3377	*njIs130[ser-2(2)p::flp, ntr-2p::frt::tomm-20(N'-55AA)::miniSOG, ges-1p::nls-GFP] (X)*		95.5
IK3178	*njIs106[odr-2(18)p::cz::caspase-3(p17), nep-2p::caspase-3(p12)::nz, ges-1p::nls-GFP] (III)*	SMBD/V ablation	53.3
IK3326	*njIs127[flp-22p::cz::caspase-3(p17), lgc-55p::caspase-3(p12)::nz, ges-1p::nls-GFP] (V)*	SMDD/V ablation	75.2
IK3376	*njIs129[lgc-55p::flp, flp-22p::frt::tomm-20(N'-55AA)::miniSOG, ges-1p::nls-GFP] (I)*		95.9

Table S2. Cell-silenced strains used in this study.

Strain name	Genotype	Experiment
CX14370	*kyEx4568[tag-168p::HisCl1::SL2::GFP, myo-3p::mCherry]*	Panneuronal silencing
IK3589	*njEx1545[gcy-8p::HisCl1::SL2::GFP, ges-1p::nls-TagRFP]*	AFD silencing
IK3590	*njEx1546[gpa-4p::flp, gcy-27p::frt::HisCl1::SL2::mCherry, ges-1p::nls-GFP]*	ASI silencing
IK3591	*njEx1547[ceh-36p::HisCl1::SL2::GFP, ges-1p::nls-TagRFP]*	AWC silencing
IK3592	*njEx1548[ins-1p::flp, gcy-28dp::frt::HisCl1::SL2::mCherry, ges-1p::nls-GFP]*	AIA silencing
IK3593	*njEx1549[aptf-1p::flp, inx-1p::frt::HisCl1::SL2::mCherry, ges-1p::nls-GFP]*	AIB silencing
IK3594	*njEx1550[AIYp::HisCl1::SL2::GFP, ges-1p::nls-TagRFP]*	AIY silencing
IK3595	*njEx1551[odr-2(2b)p::flp, acc-2p::frt::HisCl1::SL2::mCherry, ges-1p::nls-GFP]*	AIZ silencing
IK3093	*njEx1271[glr-3p::HisCl1::SL2::mCherry, ges-1p::nls-GFP]*	RIA silencing
IK3596	*njEx1552[ser-4p::flp, sto-3p::frt::HisCl1::SL2::mCherry, ges-1p::nls-GFP]*	RIB silencing
IK3597	*njEx1553[glr-1p::flp, tdc-1p::frt::HisCl1::SL2::mCherry, ges-1p::nls-GFP]*	RIM silencing
IK3598	*njEx1554[ggr-2p::flp, nlr-1p::frt::HisCl1::SL2::mCherry, ges-1p::nls-GFP]*	RIS silencing
IK3599	*njEx1555[flp-18p::flp, nmr-1p::frt::HisCl1::SL2::mCherry, ges-1p::nls-GFP]*	AVA silencing
IK3600	*njEx1556[opt-3p::flp, nmr-1p::frt::HisCl1::SL2::mCherry, ges-1p::nls-GFP]*	AVE silencing
IK3603	*njEx1559[mgl-1p::flp, glr-1p::frt::HisCl1::SL2::mCherry, ges-1p::nls-GFP]*	RMD/D/V silencing
IK3604	*njEx1560[ser-2(2)p::flp, ntr-2p::frt::HisCl1::SL2::mCherry, ges-1p::nls-GFP]*	RMED/V silencing
IK3602	*njEx1558[odr-2(18)p::flp, nep-2p::frt::HisCl1::SL2::mCherry, ges-1p::nls-GFP]*	SMBD/V silencing
IK3601	*njEx1557[lgc-55p::flp, flp-22p::frt::HisCl1::SL2::mCherry, ges-1p::nls-GFP]*	SMDD/V silencing

Table S3. Strains carrying cell markers or calcium indicators used in this study.

Strain name	Genotype	Experiment
IK0673	*njIs2[nhr-38p::GFP, AIYp::GFP] (V)*	AFD/AIY marker
IK2952	*njIs86[sra-6p::GFP] (X)*	ASI marker
IK2811	*njIs82[ceh-36p::GFP, glr-3p::GFP] (I)*	AWC/RIA marker
IK3237	*njIs112[gcy-28dp::GFP] (X)*	AIA marker
IK2711	*njIs63[odr-2(2b3a)p::GFP] (I)*	AIB marker
IK2672	*njIs39[acc2-p::TagRFP] (I)*	AIZ marker
IK2951	*njIs85[sto-3p::GFP] (X)*	RIB marker
IK2881	*njIs83[tdc-1p::GFP] (X)*	RIM marker
IK3239	*njIs114[unc-47p::flp, ser-4p::frt::TagRFP] (IV)*	RIS marker
IK3246	*njIs119[npr-4ap::GFP] (V)*	AVA marker
ST401	*ncIs401[opt-3p::ArchT::GFP, acd-4p::GFP]*	AVE marker
IK3087	*njIs94[rig-5ap::GFP] (V)*	RMD/D/V marker
IK3047	*njIs88[unc-47p::GFP] (II)*	RMED/V marker
IK3148	*njIs102[odr-2(18)p::GFP] (IV)*	SMBD/V marker
IK3147	*njIs101[lad-2p::flp, flp-22p::frt::TagRFP] (III)*	SMDD/V marker
IK3333	*njEx1389[gcy-8p::YCX1.6]*	AFD imaging
IK0961	*njIs24[gcy-8p::GCaMP3, gcy-8p::TagRFP] (I)*	
IK3329	*njEx1385[ceh-36p::YCX1.6]*	AWC imaging
IK1257	*njEx556[ceh-36p::GCaMP3, ceh-36p::TagRFP]*	
IK3330	*njEx1386[aptf-1p::flp, inx-1p::frt::YCX1.6]*	AIB imaging
IK3477	*njEx1484[aptf-1p::flp, inx-1p::frt::GCaMP6f, inx-1p::frt::TagRFP]*	
IK3487	*njIs80; njEx1484*	
IK3486	*njIs79; njEx1484*	

Movie S1. Thermotaxis behavior is accomplished within 30 minutes. Each dot represents the centroid of the animal during the thermotaxis assays in the $T<T_c$ condition (left panel) and in the $T>T_c$ condition (center panel). The time course of TTX indices in the $T<T_c$ condition (blue line) and in the $T>T_c$ condition (red line) are shown in the right panel.

Movie S2. Thermotaxis simulation reproduces the population behavior in the assays. Each dot represents the centroid of the animal during the thermotaxis assays in the $T<T_c$ condition (left upper panel) and in the $T>T_c$ condition (left lower panel). The animals in the thermotaxis simulation are shown in the center column. The time courses of TTX indices in the experiments (colored lines) and in the simulations (black lines) are shown in the right column.

Dataset S1. Thermotaxis behavior and regulation of behavioral components under different thermal contexts.

Dataset S2. Thermotaxis migration and isothermal tracking in cell-ablated/silenced animals.

Dataset S3. Thermotaxis behavior simulation, in which the data of the individual behavioral components are manipulated.

Dataset S4. Time course of the regulations of the reversal turns in cell-ablated/silenced animals.

Dataset S5. Time course of the regulations of the curves in cell-ablated/silenced animals.

Dataset S6. Time course of the regulations of the shallow turns in cell-ablated/silenced animals.

Dataset S7. Time course of the regulations of the omega turns in cell-ablated/silenced animals.

Dataset S8. Time course of the regulations of the speeds in cell-ablated/silenced animals.

Dataset S9. Calcium imaging of AFD, AWC, and AIB in immobilized animals.

References

1. Brenner S (1974) The genetics of *Caenorhabditis elegans*. *Genetics* 77(1):71–94.
2. Chelur DS, Chalfie M (2007) Targeted cell killing by reconstituted caspases. *Proc Natl Acad Sci U S A* 104(7):2283–8.
3. Qi YB, Garren EJ, Shu X, Tsien RY, Jin Y (2012) Photo-inducible cell ablation in *Caenorhabditis elegans* using the genetically encoded singlet oxygen generating protein miniSOG. *Proc Natl Acad Sci U S A* 109(19):7499–504.
4. Davis MW, Morton JJ, Carroll D, Jorgensen EM (2008) Gene activation using FLP recombinase in *C. elegans*. *PLoS Genet* 4(3):e1000028.
5. Pokala N, Liu Q, Gordus A, Bargmann CI (2014) Inducible and titratable silencing of Caenorhabditis elegans neurons in vivo with histamine-gated chloride channels. *Proc Natl Acad Sci* 111(7):2770–2775.
6. Beverly M, Anbil S, Sengupta P (2011) Degeneracy and neuromodulation among thermosensory neurons contribute to robust thermosensory behaviors in *Caenorhabditis elegans*. *J Neurosci* 31(32):11718–27.
7. Ito H, Inada H, Mori I (2006) Quantitative analysis of thermotaxis in the nematode *Caenorhabditis elegans*. *J Neurosci Methods* 154(1–2):45–52.
8. Swierczek NA, Giles AC, Rankin CH, Kerr RA (2011) High-throughput behavioral analysis in *C. elegans*. *Nat Methods* 8(7):592–8.
9. Yamaguchi S, et al. (2018) Identification of animal behavioral strategies by inverse reinforcement learning. *PLOS Comput Biol* 14(5):e1006122.
10. Pierce-Shimomura JT, Morse TM, Lockery SR (1999) The fundamental role of pirouettes in *Caenorhabditis elegans* chemotaxis. *J Neurosci* 19(21):9557–69.
11. Iino Y, Yoshida K (2009) Parallel use of two behavioral mechanisms for chemotaxis in *Caenorhabditis elegans*. *J Neurosci* 29(17):5370–80.
12. Kim D, Park S, Mahadevan L, Shin JH (2011) The shallow turn of a worm. *J Exp Biol* 214(Pt 9):1554–9.
13. Schild LC, Glauser DA (2013) Dynamic switching between escape and avoidance regimes reduces *Caenorhabditis elegans* exposure to noxious heat. *Nat Commun* 4:2198.
14. Biron D, Wasserman S, Thomas JH, Samuel ADT, Sengupta P (2008) An olfactory neuron responds stochastically to temperature and modulates *Caenorhabditis elegans* thermotactic behavior. *Proc Natl Acad Sci U S A* 105(31):11002–7.
15. Tsukada Y, et al. (2016) Reconstruction of Spatial Thermal Gradient Encoded in Thermosensory Neuron AFD in *Caenorhabditis elegans*. *J Neurosci* 36(9):2571–81.
16. Kimura KD, Miyawaki A, Matsumoto K, Mori I (2004) The *C. elegans* thermosensory neuron AFD responds to warming. *Curr Biol* 14(14):1291–5.
17. Yoshida A, et al. (2015) A glial K(+) /Cl(-) cotransporter modifies temperature-evoked dynamics in *C. elegans* sensory neurons. *Genes Brain Behav*. doi:10.1111/gbb.12260.